[Ge Nanowires Anode sheathed with Amorphous Carbon for Rechargeable Lithium batteries]

[Min-Ho Seo]

[Interdisciplinary School of Green Energy]
Graduate School of UNIST

[Ge Nanowires Anode sheathed with Amorphous Carbon for Rechargeable Lithium batteries]

A thesis
submitted to the Interdisciplinary School of Green Energy
and the Graduate School of UNIST
in partial fulfillment of the
requirements for the degree of
[Master of Science]

[Min-Ho Seo]

01.13. 2011 [Month/Day/Year of submission]
Approved by

_____

Major Advisor
[Jaephil Cho]

[Ge Nanowires Anode sheathed with Amorphous Carbon for Rechargeable Lithium batteries]

[Min-Ho Seo]

This certifies that the thesis of [Min-Ho Seo] is approved.

01.13. 2011

[signature]

Thesis supervisor: [Jaephil Cho]

[signature]

[Soojin Park]

[signature]

[Kyu Tae Lee]

Abstract

The composite electrode composed of single crystalline Ge NWs sheathed with amorphous carbon showed excellent electrochemical properties of large reversible capacity, high coulombic efficiency, excellent rate capability and stable cycle performance. c-Ge NWs synthesized by using thermal decomposition of C_2H_2 gas at 700 °C under Ar atmosphere after SLS (solution-liquid-solid) growth were found to have good performance during cycling with Li. The rate capability for charging was shown reversible capacity of 963 mAh/g with a coulombic efficiency of 90% and 700 mAh/g at the rate of 6C (= 4800mA/g). Capacity retention after 100 cycles was 72% at the rate of 0.5C. The improved electrochemical performance of c-Ge-NWs fabricated in our experiment was attributed to the formation of amorphous Ge NWs during cycling and a homogenous carbon coating on Ge NWs. Thus, these results suggest that the use of nanowires structure can be promising for alloy anode materials in lithium ion batteries.

Contents

List of figures

List of tables

Nomenclature (Scheme)

I. Introduction

1.1. Anodes materials

Many studies have been devoted to the development of high capacity lithium alloy anodes using materials such as Si, Ge, Sn and Sb to replace graphite (which has a reversible capacity of 372 mAh/g).[1-6] Si and Ge showed specific capacities of 4,200 mAh/g and 1,650 mAh/g, respectively, when forming the $Li_{22}M_5$ alloy.[7, 8] Important requirements for useful alternative materials include not only a large reversible capacity but also a high coulombic efficiency, a low potential such as that offered by graphite, a good rate capability and a stable cycle life. Alloy materials look promising due to their high reversible capacity but still do not meet all those demands. In particular, they have showed poor cycle life caused by the electrical contact loss of active materials from the current collector due to large volume changes during de/alloying with lithium. Si, for example, has the largest theoretical capacity but have had limited application due to large volume changes during lithium insertion and extraction.[9, 10] To minimize such volume strain during charge and discharge, strategies for versatile morphology control using 0D nanoparticles, 1D nanowires, and 3D-particles have been reported.[2, 5, 11-17] Among those morphologies, nanowires are considered to be attractive due to good electronic conduction along the length of each wire, short lithium ion diffusion distance, and high interfacial contact area with electrolytes.[4, 18] The initial alloying process of metal catalysts, growth of nanowires nuclei, changes in nanowires shapes and diameters as well as deposition of source materials are described by many works previous. In particular, Si nanowires among these researched have been studied extensively as anode materials, but Ge nanowires have not been the focus of much research. Various novel technologies such as vapor–liquid–solid (VLS) process (also known as metal catalytic growth), Supercritical fluid-Liquid-Solid (SFLS) method and Solution-Liquid-Solid (SLS) method are well known. These methods can produce free-standing crystalline nanowires of semiconductor and metal oxide materials with fully controlled nucleation sites and diameters from pre-formed metal catalysts. Since the 1960s, semiconductor whiskers grown by this technique[19, 20] have been extensively studied. In recent years, various new techniques have been developed to realize 1D nanostructures, such as laser-assisted chemical vapor deposition (CVD)[21], Laser ablation[22], thermal CVD[23]. Although the number of various kinds of 1D nanostructures fabricated via different techniques increases dramatically every year, our understanding of the basic process of 1D nanostructure formation has not reached maturity. The methods to fabricate desired 1D nanomaterials with tailored atomic structures and to integrate functional nanostructures into devices are still challenging issues for materials scientists.

1.2. The problem of anodes materials

It is formed protect layer at the negative electrode which is electronically insulating and thus hinder further electrolyte reduction but still act as a pathway for the active charge carrier, the lithium cation (Scheme. 1).

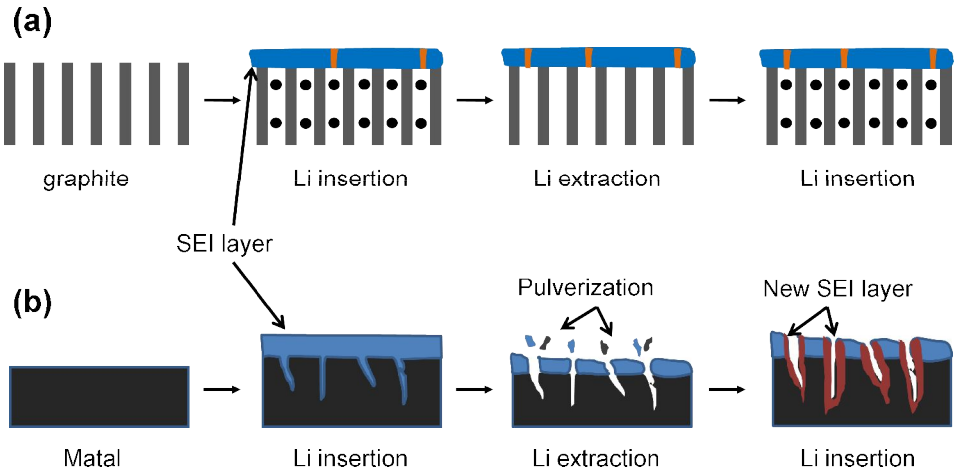

Scheme 1. The comparison of carbonaceous SEI and metallic host materials one.

In other words, these layers are called a solid electrolyte interphase (SEI). Since the SEI formation is associated with the irreversible consumption of material (lithium and electrolyte), the corresponding charge loss is called irreversible capacity. The irreversible capacities have to be minimized because they are detrimental to both specific energy and energy density of the cell and, moreover, increase the material expenses due to the necessary excess of costly positive electrode material which is the lithium source after cell assembly. By way of illustrative examples, special emphasis will be put on new electrolyte additives and reactions taking place at the lithium storage alloy interface.

In order to overcome the problems with the mechanical disintegration of lithium storage metals and alloys by new SEI formation on lithium storage metals, several simple strategies for the design of the metallic host materials have been suggested. These strategies are as follows: (a) Proper design of particle morphology, especially particle size and porosity. For instance, a critical-size material below which cracking does not take place on volume changes during Li insertion/extraction. The equation of critical grain size is given as follows[24] :

$$d_{crit} = 32.2\gamma(1-2\nu)2V_0^2/E\Delta V^2$$

(d_{crit}: critical grain size, γ: surface energy, ν: poisson's ratio, V_0: initial volume, ΔV: volume change, E:

elastic modulus)

However, this equation has a significant problem. For instance, if this equation is calculated for $Li_{4.4}Si$ ($\Delta V/ V_0$=3.12) yields, it is predicted $d_{crit} \approx 0.0014$ nm. These results reveal that it's almost impossible to synthesize the grain size to prevent pulverization during Li alloying, because the predicted critical grain size is less than the unit cell size. Pores in the original material should offer additional space for expansion and therefore also increase the cycling stability[17, 25, 26]. Cho *et al*[27] reported porous silicon anode materials. 3D-porous Si particle, mesoporous Si nanowires and Si nanotubes showed the improved performance of the capacity and cycle life. The average particle size of silicon is 30 nm, its charge capacity is 3311 mAh/g and the capacity retention after 5 cycles revealed only 5%. Mesoporous Si nanowires have an initial charge 3163 mAh/g with an initial coulombic efficiency of 86%. The capacity after 80 cycles was 2738 mAh/g, which corresponds to 87% capacity retention. The Si nanotube also showed the improved cycle performance by using full cell consisting of a $LiCoO_2$-based cathode and a Si nanotube-based anode. The initial capacity at rates of 3C and 5C was above 3000 mAh/g, and capacity retention after 200 cycles was 89% at a rate of 1C.
(b) Incorporation of inactive components the dilution of the active material with matrix components results in an increased cycling stability, since the reacting and expanding phase is stabilized by the no-reacting inactive matrix (Scheme 2). The mixed-conductor matrix concept has been demonstrated by Huggins *et at*[8]. The drawback of these active/inactive composites[28] is that the presence of inactive matrix components reduces the specific charge as well as the charge density of the electrode material.

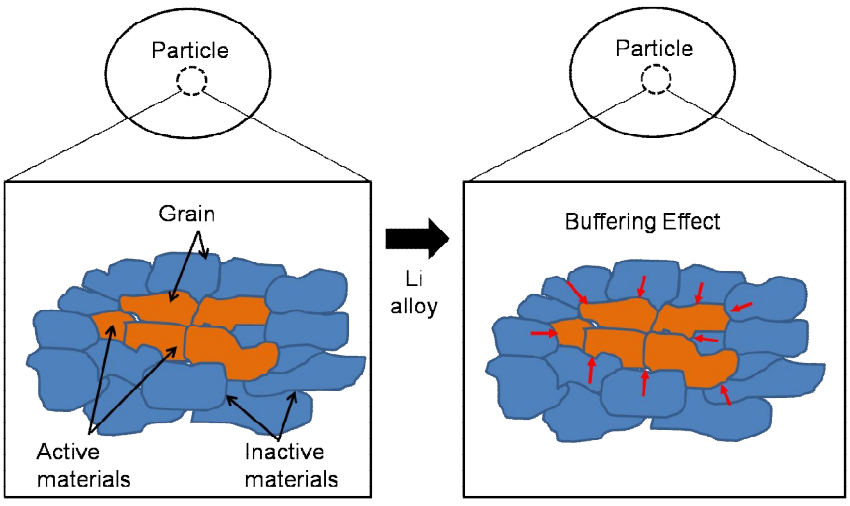

Scheme 2. The illustration of active/inactive composite.

(c) Use of multi-phase instead of single-phase materials in multi-phase materials like e.g. $Sn/SnSb_5$ or $Sn/SnAg_3$[29, 30], the single components usually react one at a time. Hence, while one component is reacting (expanding or contracting), the other does not take part in the reaction.

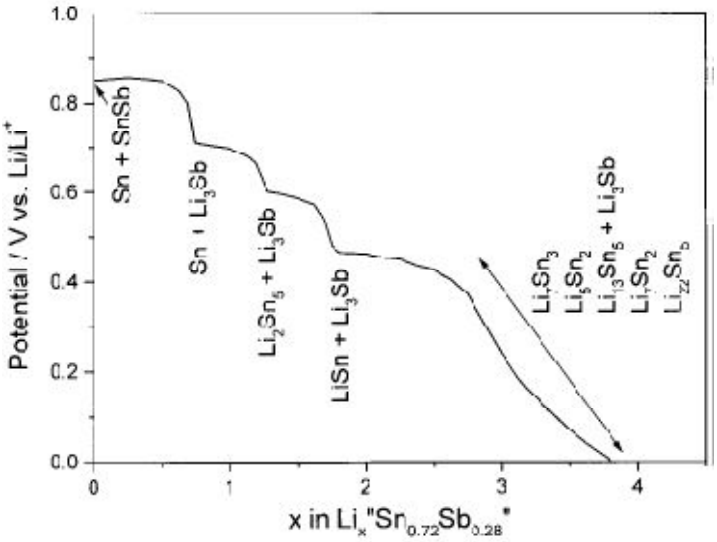

Figure 1. Discharge curve of electroplated Sn/SnSb[31].

1.3. Germanium electrode for lithium ion batteries

Recently, commercial batteries use graphites as anode materials, However, there is strong interest to replace carbons by anode materials which can show even higher specific charges/charge densities (Figure 2).

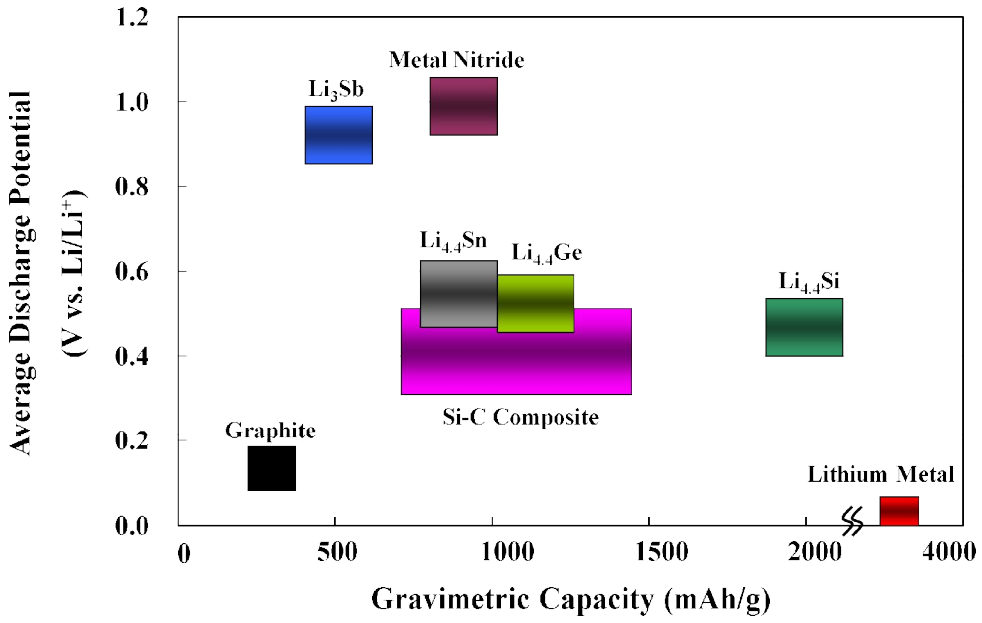

Figure 2. The specific capacity of group IV elements[31].

The replacement of graphite by lithium alloys has been under investigation since Dey *et al*[32]

demonstrated the feasibility of electrochemical formation of lithium alloys in liquid organic electrolytes in 1971. A large number of metals and intermetallics (alloys), such as Ge, Si, Sn, Sb, and SnSb etc., are capable of reversible accommodation of lithium. The Germanium material among these research are not well-studied as silicon, because of their thermal unstability. In fact, but the diffusivity of lithium in germanium is higher than that of silicon (above 5 times)[33], and bond energies of Ge-X bonds are generally considered to be about 10% less than corresponding Si-X bonds. This means that the synthesis of Ge is easier than Si one. Unfortunately, the insertion and extraction of Li are accompanied by significant volume changes (e.g. from Ge to $Li_{22}Ge_5$: ~400% volume increase; by comparison, from graphite to LiC_6: only ~10% volume increase), which in the case of ordinary coarse-grained, bulk metal host materials leads to cracking and crumbling of the electrode and hence renders an application in rechargeable batteries impossible.

Table 1. The electrochemical performance of Germanium electrode.

Morphology (size)	Precursors	Process	Specific Capacity (mAh/g)		Cycling retention		Coulmbic efficiency (%)	C-rate	Ref.
			1st discharge	1st charge	Capacity (mAh/g)	Cycle number			
Nanowire (50~100 nm)	GeH_4	CVD[1)]	2967	1141	~1000	20	39	0.05C	4
Thin Film (~250 nm)	Ge powder	PVD[2)]	~2400	~1600	1700	60	~66	0.25C	34
Particle (12 nm)	Ge powder	PVD*[3)]	~2400	~1200	~800	60	~50	0.25C	34
Meso Porous (500 nm)	GeO_2, Mg powder	Mechano-chemical[4)]	2155	944	789	20	44	0.1C	35
0D hollow (220 nm)	$GeCl_4$	Template etching[5)]	1428	1380	1162	100	~95	0.5C	3
3D porous (20 nm)					1415	100			
amorphous particle (~10 nm)	$GeCl_4$	Sol-gel[6)]	1441	1067	1290	30	74	0.2C	36
Nanoparticle (~20 nm)	TA-Ge	Solid-state pyrolysis[7)]	1109	923	900	50	77	0.1C	37
Particle (~5 μm)	Copper(II) D-gluconate, Ge,Cu powder,	Pyrolysis-ball-milling[8)]	962	754	530	50	78.4	0.1C	38

1) CVD : Chemical vapor deposition, 2) PVD : Physical vapor deposition using evaporation, 3) PVD*: Modifying method of PVD by forming gas, 4) Mechanochmical reaction : The method of etching after redox reaction of GeO_2, Mg power mixed by ball-milling, 5) Template etching (sol-gel) : the method of etching between spherical silica nanoparticle and ethyl-capped Ge gel by HF solution, 6) Sol-gel : the method of buthyl group capping by buthyllithium, 7) Solid-state pyrolysis, thermally polymerizing, 8) Pyrolysis and mechanical milling process : the method of mixing Cu_3Ge with Ge, Cu powder by HEMM process after synthesis of Cu/C.

II. Growth methods for Germanium nanowires

2.1. Vapor-Liquid-Solid (VLS) method

One of the most common synthesis method used for nanowires is the vapor-liquid-solid growth process, which is first discovered by Wagner and Ellis[20] in 1964. They used Au particles as catalysts to grow crystalline whiskers from vapor sources such as $SiCl_4$. The fundamental theory for Si nanowires growth is schematically shown in Scheme 3.

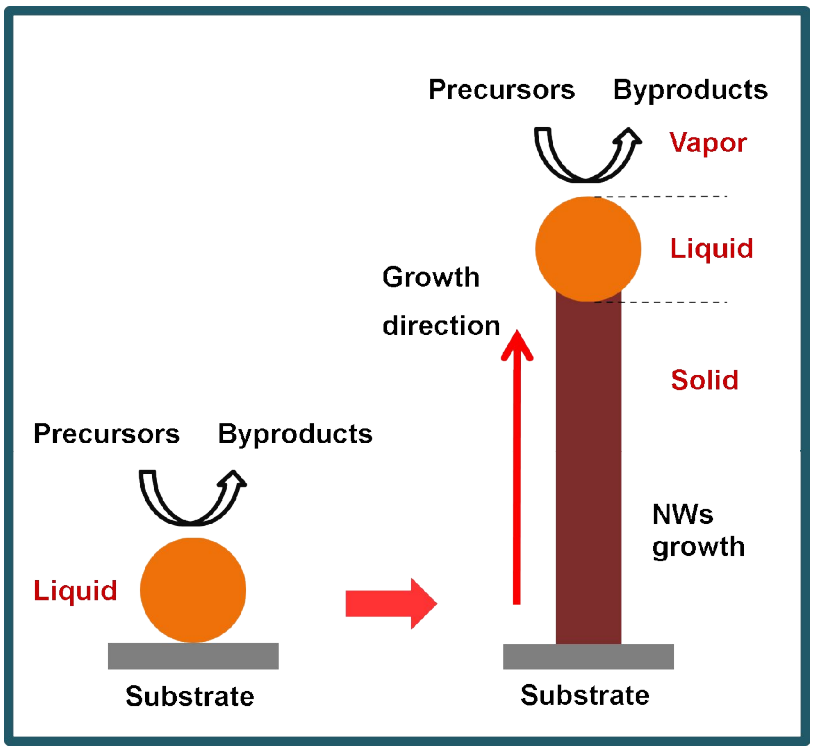

Scheme 3. The process of VLS method.

The Au particles first used as a catalyst to form a liquid alloy droplet on the surface of a substrate. In addition, the whisker grows by precipitation of silicon from the liquid alloy droplet (Au-Si). As shown in Figure 3, the eutectic point of the alloy in the binary phase diagram (Au-Si) is very low (about 360

ºC at an Au:Si ratio of 4:1) compared with the melting temperature of Au or Si. According to binary phase diagram, the alloying reaction of Au and Si are possible to form a solid solution from all silicon content (1~100%).

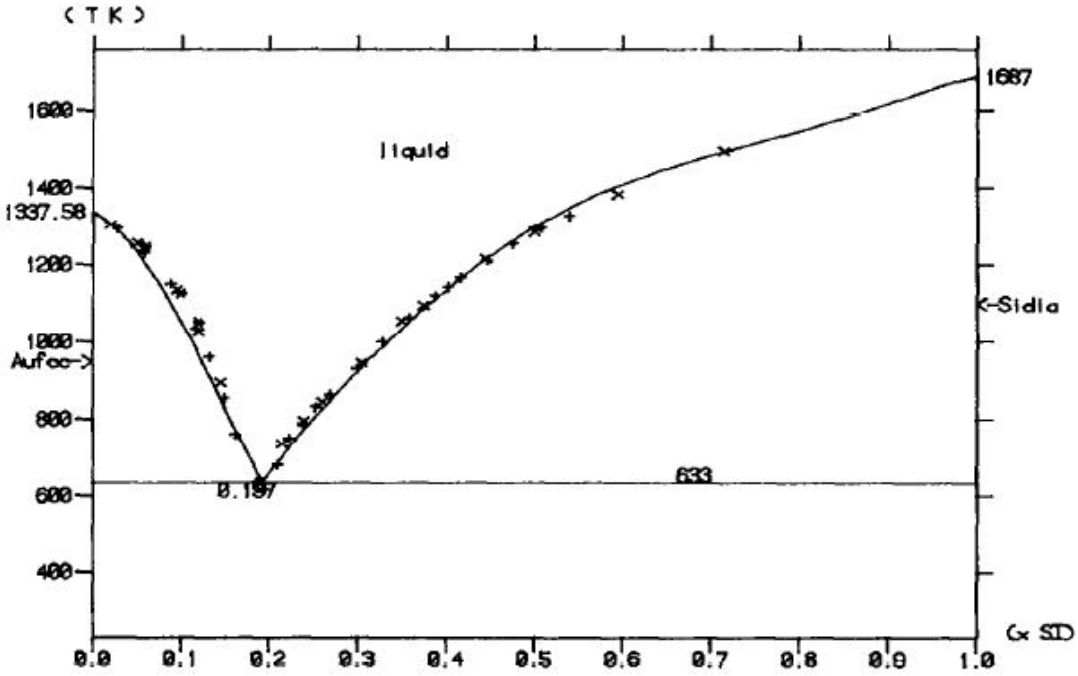

Figure 3. The Gold-Silicon binary alloy phase diagram[39].

In the case of Si deposition from the vapor mixture of $SiCl_4$ and H_2, the reaction between $SiCl_4$ and H_2 happens at a temperature above 1000 ºC without catalysts. Below this temperature, almost no deposition of silicon occurs on the substrate surface. At a temperature above 363 ºC, Au particles and Si atoms can form Au-Si eutectic droplets on surfaces, and the reduction of silicon atom happened alloying of the Au-Si droplets by a catalytic effect. The Au-Si droplets of binary material absorbed silicon atom from the vapor phase by a supersaturated state. The nanowires grow only in the areas seeded by metal catalysts, and their diameters are determined by the sizes of the catalysts. The result can be known from the previous research[40]. It has recently become a widely used method for synthesizing a variety of 1D nanomaterials that include elemental semiconductors[18, 20, 41-43]. Germanium is also an important semiconducting material with high mobility and a band gap of approximately 0.6 eV. Germanium nanowires were first reported by Heath group about ten years ago, synthesized by using a solvothermal approach.[44] Also, Germanium nanowires have been synthesized by using VLS methods. Wu *et al.*[23] reported that Ge nanowires were synthesized by using vapor transport. Both Ge powder and GeI_4 mixture was added in tube and a gold coated (001) Si substrate. The substrate was coated with gold thin films using sputtering system, and was then sealed and heated to 1000-1100 ºC. During the transport of the precursors, the following reaction occurs at high-

temperature zone:

$$Ge(s) + GeI_4(s) \rightarrow 2GeI_2(g)$$

The GeI_2 vapor is then transported to the cold end of the quartz tube, and it is condensed into the gold islands on the heated substrate. Finally, it is disproportionated according to

$$2GeI_2(g) \rightarrow Ge(l) + GeI_4(g)$$

It was found that the substrate surface was covered with pure nanowires with diameters ranging from 5 to 300 nm. Wang *et al.*[45] reported low-temperature growth of GeNWs. The synthesis of single-crystal germanium nanowires prepared by the CVD of germane (GeH_4) at 275 ºC under atmosphere pressure with Au nanocrystals as seed particles. The nanowires growth is only obtained by controlling the GeH_4 decomposition through H_2 addition. Germane occur thermal decomposition by the following routes:[46]

$$GeH_4 \rightarrow GeH_2 + H_2$$
$$GeH_2 \rightarrow Ge + H_2$$

The methods of growth are limited by the efficient GeH_4 pyrolysis and low eutectic temperature for Ge and Au seeds. The phase diagram suggests that over a wide range of temperatures above 360 ºC (the eutectic temperature), a VLS-type process can take place if the concentration of Ge is increased within the Au particle. However, germanium nanowires are actually formed lower temperature than the eutectic temperature (~275 ºC) by about 85 ºC, and the melting temperature of the Au-Ge alloy is significantly suppressed by Au nanoparticles from macroscopic Au. Nanomaterials such as Au often exhibit lower melting temperature than bulk materials[47]. The decreased melting point for the Au-Ge cluster is an important factor for the growth of Ge nanowires (~23 nm) at this temperature. Instead of controlling the growth direction of nanowires via epitaxy, Jagannathan *et al*[48] reported that the nanowires were produced through oriented cylindrical mesopores as template which consists of organosilicate. A polystyrene (PS) and poly(ethylene oxide) (PEO)(PS-b-PEO) and silsesquioxane (SSQ) are used as the organic block copolymer and the inorganic precursor for template precurosr, respectively. The length of template consisting of block copolymers and the block copolymer/SSQ mixture determine the final morphology of the film. Therefore, to obtain nanowires through mesoporous materials need to form the catalyst inside the pores. Gold catalyst film was deposited by using electron beam evaporation onto a silicon wafer having layer of thermal oxide. After the treatment of silicon wafer and template synthesis, the samples were loaded in a cold wall, lamp heated,

chemical vapor deposition nanowires growth system. Chan *et al.*[4] reported the synthesis of Germanium nanowires directly onto metal current collector substrates for anode in Li-ion battery. Scheme 4 shows difference from current manufacturing press which of the previous battery electrode. Slurry for battery contains the active material with conducting carbon (carbon black) and polymeric binder onto the current collector (such as Cu and Al foil). The nanowires of Scheme 4(b) directly grew onto current collector without conducting carbon. The germanium nanowires were synthesized in a tube furnace by using VLS method. Stainless steel with gold film as catalyst was used for current collector and substrate to grow germanium nanowires.

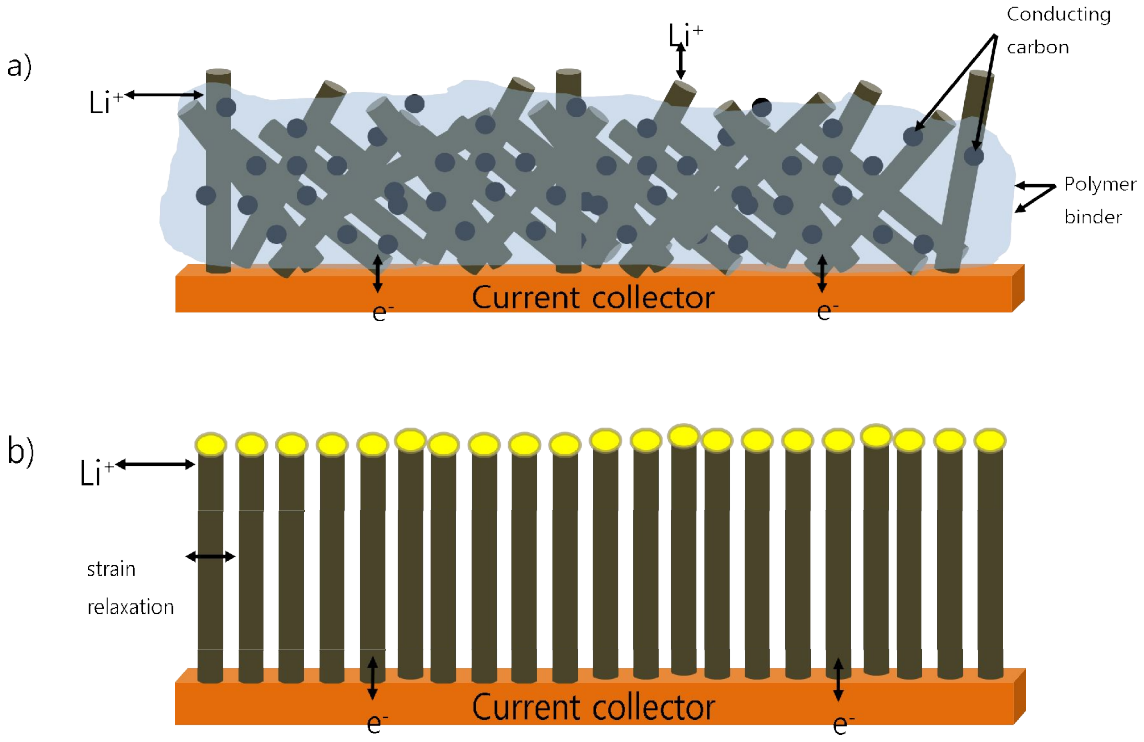

Scheme 4. (a) A traditional battery electrode consisting of a composite of active material (rods), conducting carbon to enhance conductivity (black circles), and a polymeric binder. (b) NW electrode design consisting of NWs grown directly on the current collector.

The gold particles on the tips of the NWs are the catalyst used in the synthesis. Advantages of this electrode design include good electrical contact between the current collector, good charge transport along the length of the NW, facile fabrication, and no need of additives. The main objective of using gold as a catalyst exhibits a low bulk eutectic temperature (363 ºC) and no stoichiometric compounds. However, the Au catalyst presents a significant problem for integrating nanowires into the mainstream semiconductor process, because Au plays a role of a contaminant and offers no useful properties to the nanowires after growth. Au can also diffuse into Si nanowires during the growth.[49] Therefore, new

non-contaminating catalyst schemes need to be explored to facilitate the integration of Ge nanowires into applications. Thus, Ge nanowires using manganese germanide seeds are reported by Lensch-Falk *et al.*[50] This research of germanium nanowires have three merits compared to previous approaches: 1) The nanoparticle using seeds are not noble metal (such as Au), avoiding the potentially negative influence on electrical properties, 2) The vapor-phase deposition and self-assembly of the seed greatly simplifies the nanowires synthesis process, 3) The self-assembled seed naturally produces a narrow distribution of nanowires diameters. The crystalline Ge nanowires growth from gas-phase precursor can be attributed to the formation of the manganese germanide from the Mn particles in the presence of GeH_4. Especially, the growth occurs at 370 ºC below the lowest eutectic point on the Mn-Ge binary phase diagram. Sun *et al*[51] reported that another possible alternatives are indium (In) and antimony (Sb), both of which are front-end materials, commonly used for channel or shallow junction doping of complementary metal-oxide semiconductor (CMOS) field-effect transistor. To investigate the fundamental possibility of a VLS growth with In and Sb as the catalyst, it's known the materials contained by Figure 4.

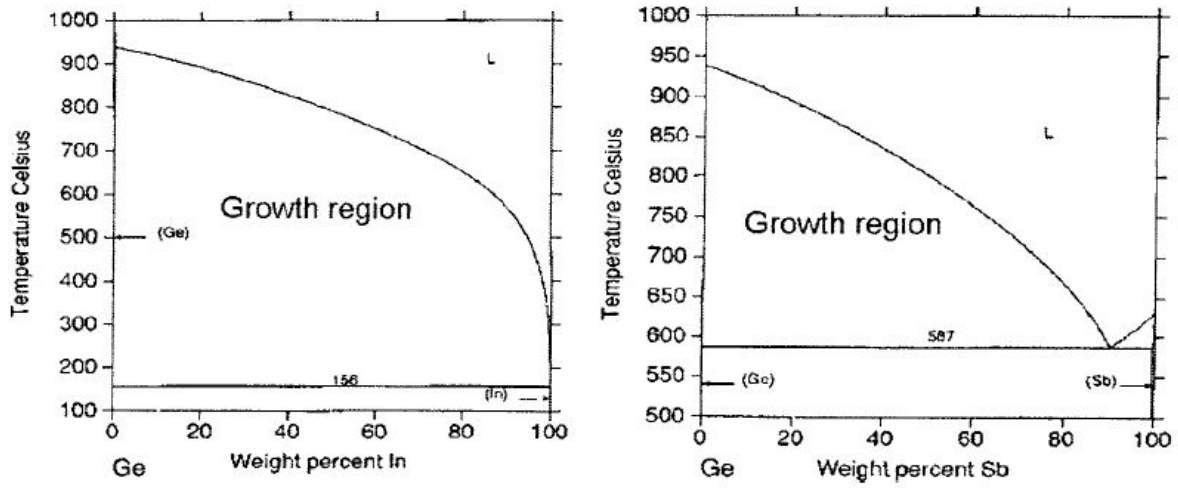

Figure 4. Indium germanium binary alloy phase diagram (left) and antimony germanium binary alloy phase diagram (right). The eutectic temperatures for the In–Ge and Sb–Ge alloy systems are 158 and 587 °C, respectively.

In and Sb also exhibit eutectic behavior with Ge, similar to Au. In particular, indium has a very low melting point (156 ºC) as the eutectic temperature with Ge. There exist no stoichiometric compounds in either Ge–In or Ge–Sb binary systems. The low solid solubility of Ge in both metals may affect the time for supersaturation and facilitating the axial growth. The substrates were sputtered with In and Sb catalyst films. The substrate with the catalyst was loaded downstream into the low temperature zone as the target substrate for nanowires growth. Ge vapor dissolved into the In (Sb) particles and

formed liquid alloy at the above eutectic temperature. The continuous feeding of the source material increased Ge concentration inside the droplets. Finally, when supersaturation reached, precipitation and axial growth of nanowires occurred according to VLS mechanism. The morphology of Germanium nanowires are better in In and Sb catalyzed system than that of Au-catalyzed ones, resulting in the spheroidization of nanowires. However, the temperatures used here may not provide sufficient energy for the atoms to migrate into independent spheres, compared to the spheroidization of Si nanowires at relatively higher temperatures. Also, one dimensional germanium nanowires have been directly synthesized on a thin insulating (SiO_2) layer by using metallic indium or antimony as catalyst by VLS approach. The characterization of nanowires synthesized from this catalyst revealed no simultaneous doping except for the presence of the In or Sb beads at the tip. Due to the low solubility of In and Sb in Ge, high temperature annealing is typically required for doping In and Sb into Ge or Si. At the nanowires growth conditions in this work, the amount of In and Sb in the nanowires cannot reach the dopant concentrations.

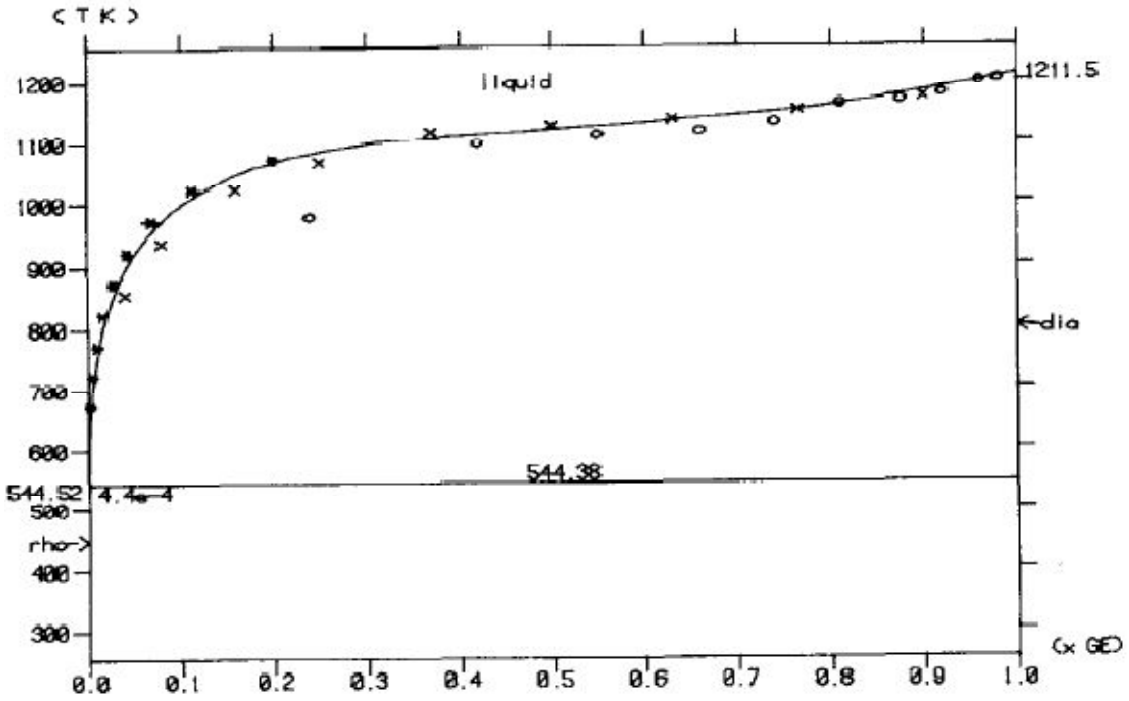

Figure 5. The Bismuth-Germanium alloy phase diagram[52].

Yan *et al.*[53] reported the synthesis of high quality single crystalline Ge nanowires by using Bi as the catalysts via an in situ catalyst evaporation method. Bismuth, germanium, and carbon powders were used for synthesis of the nanowires. Copper grids coated with holey carbon film were placed at the lower temperature region to collect the products. Large quantities of nanowires can be observed with diameters in the range of 10-40 nm. The effect of Bi/Ge molar ratio was investigated through

controlled experiments using source materials with different Bi contents. If large amounts of Bi were used, micrometer-size Bi particles would be condensed at the low temperature region on the substrate instead of Ge nanowire growth. Both the yield and purity of the nanowires could be improved when source material with a Bi/Ge ratio of 0.05/1 was used. The density of the nanowires started to decrease when the molar ratio was even lower. A proper Bi content in the source materials is critical to ensure the formation of small Bi particles with desired densities, which later serve as catalyst particles for Ge nanowires growth. The growth process of the Ge nanowires with Bi catalyst can be explained by the VLS mechanism. The melting point of Bi (271.3 °C) is shown much lower than that of Ge (936.3 °C) by binary phase diagram (Figure 5); thus, it can expect Bi to evaporate first when the furnace was heated to 1000 °C. Liquid droplets of Bi are condensed on the substrate collector when Bi vapor was exposed to lower temperature region (300 °C) in Ar flow. Ge vapor concentration would increase significantly when the temperature was increased above its melting point (936.3 °C). Continuous adsorption of Ge vapor to the Bi droplet surface resulted in axial nanowires growth after the alloy droplets reach supersaturation. Usually the metal catalyst particles or thin films are first deposited on the substrate surface before loading into the furnace for nanowires growth. The Bi catalyst particles are condensed at the low temperature region from the vapor generated via in situ evaporation process. This one-step catalyst deposition and nanowires growth process are used for preventing the oxidation of Bi nanoparticles by Ar protection atmosphere in the furnace during growth. Also, the carbon added in source materials plays the role of removing the residual oxygen in the furnace chamber and maintain reduction conditions. Bi is a good candidate for Ge nanowires synthesis since there are no stoichiometric compounds in Bi-Ge binary systems.[52] Also, the usage of Bi as catalyst for Ge nanowires growth offers two major advantages. First, the solubility of Ge in Bi remains quite low for growth temperatures up to 700 °C. Second, the low eutectic temperature of Bi-Ge enables the Ge nanowires synthesis at low temperatures. The eutectic temperature of Bi-Ge (271 °C) is lower than that of Au-Ge (363 °C).

Low temperature synthesis is desirable for nanowires growth on organic substrates and for solution-phase synthesis to alleviate solvent decomposition. Ge NWs were synthesized inside a standard thermal chemical vapor deposition furnace using germane (GeH_4) as a growth precursor by Xiang *et al*[54]. The substrates were fused wafers covered with Bi, which was deposited by electron beam evaporation from a high purity source. The purpose of the annealing step was to reduce the native Bi oxide so that the Bi layer can be exposed to the source gas flow acting as a catalyst for its decomposition. For the Ge NW synthesis, the temperature was lowered and GeH_4 was introduced into the growth chamber. The tapering of the Ge NWs is characterized by a decreased NW diameter with the distance from the substrate. Aside from the Bi evaporation, tapering in NWs is due to sidewall deposition of Ge on the NW sidewall. The NW sections near the basis are exposed longer and thus grow thicker. Sidewall deposition is possible when GeH_4 is thermally decomposed and its rate

increases exponentially with temperature. At higher temperature it turns to be more substantial, explaining that tapering is observed for temperatures higher than 300°C. For temperatures higher than 400 °C, NW growth is not observed, due to the high vapor pressure of Bi.

2.2. Solution-Liquid-Solid (SLS) method

The major advantages of the solution-based technique (non-aqueous or non-hydrolytic media) for synthesizing nanomaterials are high yield, low cost and easy fabrication. The solution based technique has been demonstrated as a promising alternative approach for mass production of metal, semiconductor and oxide nanomaterials with excellent controls of the shape and composition with high reproducibility. Scheme 5 shows the process of SLS method

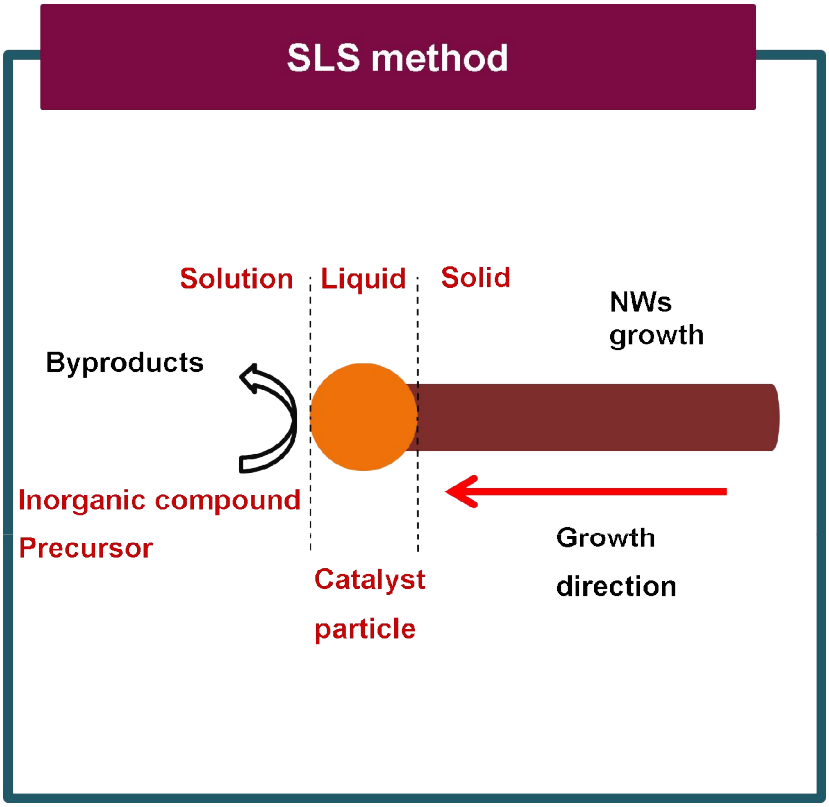

Scheme 5. The process of SLS method.

In particular, this technique is able to assemble nanocrystals with other functional materials to form hybrid nanostructures with multiple functions with great potential for applications in nanoelectronic and biological systems. The nanocrystals synthesized in aqueous media may often suffer from poor crystallinity, but those synthesized under nonhydrolytic conditions at a high temperature, in general, show much better crystal quality[55] for the formation of nanowires from solution, several routes have been developed, such as metal-catalyzed solution-liquid-solid (SLS) growth from metal seeds.[19, 43, 55-

[58] Similar to the VLS methods, during the SLS methods, monomers are generated by decomposition of molecular precursor at a high temperature. The metal catalysts for this kind of methods are extremely small and therefore easily activated at low temperatures. The monomers react with the metal nanoseeds to form supersaturated alloy droplets. Semiconductor nanowires growth, e.g., Silicon and Germanium nanowires[55, 56, 58] from Au nanocatalysts supercritical fluid environment have been achieved.

The synthesis of Germanium nanowires using SLS(solution-liquid-solid) was first reported by Heath *et al*.[44] Two liquid-solutions based on synthesis are presented for the efficient fabrication of single crystal Ge nanowires. Both are based on the high-temperature, high-pressure reduction of $GeCl_4$ and phenyl-$GeCl_3$ in a pentane or hexane solvent. Phenyl-$GeCl_3$ is employed as the size-controlling reagent. The results of this synthesis are quite enlightening, and imply that wet chemical nanofabrication may not only be applied to the control of size but to the control of shape as well. The reactions were carried out in a sealed pressure bomb made from a high-percentage nickel alloy and equipped with a magnetically coupled stir drive and the reagents were mixed dry hexane, $GeCl_4$, phenyl-$GeCl_3$, Na dispersion in toluene. The products showed a diameter of 18nm and length of 10μm. Hanrath *et al*[55] reported the solution phase synthesis of Ge nanowires using alkanethiol-capped Au nanocrystals, dispersed in cyclohexane heated and pressurized above its critical point, as the seeds for wire growth. The effects of temperature, pressure, precursor, reaction time, and precursor concentration were investigated. The optimum conditions for Ge nanowires growth are identified. The germanium precursors were tetraethylgermane (TEG) and diphenylgermane (DPG). A stock solution of Au nanocrystals in the germanium precursor (Au:Ge molar ratio 1:2000) was prepared under a nitrogen atmosphere. Nanowires growth was used seeds of 6.5 and 2.5 nm alkanethiol-capped Au nanocrystals for reactions using TEG and DPG, respectively. The average diameter of the nanowires produced from TEG was 87 nm, while DPG under the same synthesis conditions yields nanowires with an average diameter of 17 nm. Two primary factors appear to broaden the nanowires size distribution: 1) Au nanocrystal agglomeration and 2) unfavorable decomposition kinetics in the case of TEG. The injected precursor solution contains relatively size-monodisperse, sterically stabilized Au nanocrystals; however, agglomeration of nanocrystals or liquid alloy Au:Ge droplets at elevated temperatures could be expected and would subsequently lead to broad Ge nanowires diameter distributions. These results showed the possibility of the different decomposition kinetics of each precursor. TEG appears to be more kinetically stable, as much less Ge product results from the low-temperature reactions than when DPG is used. DPG can form radicals stabilized by the two phenyl substitutions, leading to an efficient disproportionation reaction and faster decomposition kinetics than TEG. The slower decomposition kinetics of TEG, on the other hand, allows more time to elapse before the nanocrystals are saturated enough to produce wires. Instead of nanowires, micrometer size spherical particles form. One explanation for particle formation at 500°C is that Ge nanowires form

initially but subsequently melt into particulates. Another explanation occurs the kinetic competition between wire growth and homogeneous Ge particle nucleation. The precursor decomposes into Ge atoms that can either dissolve into the Au:Ge droplets and crystallize into nanowires, or homogeneously nucleate into spherical particles. At temperatures below 500 °C, Ge nucleation from the liquid Au:Ge seed particles is faster than homogeneous Ge particle nucleation. However, at 500 °C, nanowires growth cannot be sustained because the Ge supply rate to the system overwhelms the nanowires crystallization rate. When the Au:Ge ratio is increased to 1:20 instead of 1:2000, the seed particles can sustain nanowires growth to a degree, respectively. The Ge nanowires synthesized in supercritical cyclohexane using gold nanocrystals as seeds exhibit crystalline cores. For example, The derived nanowires size produced from DPG at 400°C was 20 nm, which agrees well with the 17 nm average wire diameter determined. On the basis of the VLS and SLS mechanisms, one would not expect to form wires at temperatures below the eutectic temperature. However, Ge nanowires were observed to form at reaction temperatures as low as 300 °C. There are two possible explanations for this observation. Either the Au:Ge eutectic While the injection solutions used for all experiments discussed thus far contained 200 mM, complementary experiments with diluted injection solutions at 20 and 800 mM were carried out with TEG and DPG at 450 °C and 13.8 MPa. While the precursor concentration does not appear to affect the morphology of the nanowires grown with DPG, the materials obtained from the TEG experiments showed significant concentration dependence. The low concentration of TEG produces nanowires network structures very different. The quality of Ge nanowires formed from DPG is superior to that of those obtained from TEG due to the faster decomposition of the former.

Lu *et al*[56] reported GeI_2 as an effective precursor for Ge nanocrystal synthesis at 300 °C in TOP (tri-octylphisphine), with high yields and minimal organic contamination. Ge nanowires produced by injecting GeI_2 along with stabilized Bi seeds into TOP at 365 °C on a Schlenk line. The Bi nanocrystals were synthesized by room temperature reduction of bismuth(III) 2-ethylhexanoate ($Bi[OOCCH\text{-}(C_2H_5)C_4H_9]_3$) in dioctyl ether in the presence of TOP. TOP serves as a capping ligand that prevents significant nanocrystal aggregation. After injecting the precursor/nanocrystal mixture into preheated TOP, the mixture was stirred at 350°C. The Ge nanowires were obtained by using a GeI_2:Bi mole ratio of 80:1. The crystalline Ge nanowires have two key points: a) Bi-Ge binary phase has low temperature (270°C), and b) the highly reactive organic-free Ge precursor used. GeI_2 disproportionates to Ge and GeI_4 with relatively high chemical yield at temperatures greater than 330 °C below its boiling point (550 °C) and the boiling point of many widely used solvents, such as tri-*n*-octylphosphine (TOP). Control experiments where GeI_2 was injected without Bi nanocrystals into TOP at 365 °C showed Ge nanoparticle formation, indicating rapid homogeneous GeI_2 decomposition. With Bi present in the concentrations used for nanowires synthesis, Ge nanoparticles were not observed. Although small Ge clusters may nucleate homogeneously, their interfacial free

energy is greatly lowered by incorporation into the much larger 20 nm Bi particles. Heterogeneous GeI_2 decomposition on the Bi seed particle surface could also occur. Pan and coworker[59] reported the use of the sol–gel technique to prepare film-like gold/silica substrates from a solution based precursor containing tetraethoxysilane (TEOS) and hydrogen tetrachloroaurate ($HAuCl_4$). A large amount of Au nanoparticles with diameters of 50–100 nm are evenly distributed on the substrate surface, and the Ge nanowires thus prepared are straight, single crystalline, and quasi aligned. Importantly, the solution-based precursor allows locating gold/silica gel on any well-defined position on substrates by shadow mask, printing, or soft lithography methods, which could facilitate the integration of Ge nanowires for characterization and devices. Two kinds of substrates were prepared for Ge nanowires growth using two different solution precursors: a) free-standing thick films without patterning and b) thin films patterned with TEM grids. For the film without pattern, TEOS was just mixed with $HAuCl_4$ aqueous solution and ethanol by magnetic stirring. The solution was then dropped onto surface for formation of the film with thickness of about 30–50 mm. Then, the gel was dried to prevent irregular shape and detached from the surface during overnight. For the patterned film, the solution was prepared as follows: 0.4 g of Pluronic P-123 triblockcopolymer was dissolved in 10 ml of ethanol. The addition of triblockcopolymer improves the wetting ability of the solution with the silicon wafer and also increases the viscosity of the solution, thus facilitating the formation of a very thin and uniform film on a silicon wafer without cracking. The solution was then coated on the silicon wafer by dip coating to form a very thin layer. Prior to being loaded into the furnace for nanowires growth, both kinds of substrates were annealed, during which large quantities of Au nanoparticles with diameter of 50–100 nm were formed and were evenly distributed on all substrate surfaces (including the side surfaces) due to the transport of Au species from within the bulk substrate and subsequent aggregation. These Au particles act as the catalysts for Ge nanowires growth. The nanowires growth was carried out in a tube furnace system. In addition, the gold/silica substrates were placed downstream of the Ge source. The vapor generated from the Ge source was transferred to the gold/silica substrates by flowing Ar, providing Ge feedstock for Ge nanowires growth. Apparently, the nanowires grow out not only from the top surface but also from all side surfaces. The nanowires are very straight and uniform in diameter (50–80 nm). These white-grey particles newly formed nanowires with Au nanoparticles at their tips.

Chockla *et al*[58] demonstrated the SLS growth of Ge nanowires using Au nanocrystals as seeds. There are a number of solvents with boiling temperatures exceeding the Au:Ge eutectic (Table 2), including squalane (~420 ºC), octacosane (~430 ºC), dotriacontane (~460 ºC), trioctylamine (~380 ºC) and trioctylphosphine (~360 ºC). All reactions were carried out using a nitrogen-filled glovebox and a Schlenk line. Stock solutions of DPG were prepared in a nitrogen filled glove box by adding DPG with the solvent used for the reaction. For reactions in octacosane and dotriacontane, DPG stock solutions were prepared in toluene since octacosane and dotriacontane are solids at room temperature.

For SLS nanowires growth, a dispersion of Au nanocrystals in toluene were added to the DPG stock solution before injection into the reaction flask, corresponding to a Ge:Au mole ratio of 1250:1 in the injection solution. Ge nanowires could be produced by Au nanocrystal-seeded SLS growth in solvents at 380 ºC by the thermal decomposition of DPG. In the absence of Au nanocrystals, only amorphous Ge particles were formed. DPG decomposition is in fact very slow and one would not expect DPG to be a suitable reactant for SLS nanowires growth. However, when Au nanocrystals are added to the reaction, the solution turns instantaneously black due to the formation of Ge from DPG. Phenylsilanes also decompose by a similar redistribution pathway in organic solvents at elevated temperature. Significant quantities of Ge nanowires could be produced in DPG decomposes to Ge by phenyl redistribution to GeH_4 and $GePh_4$. SLS growth can be used to produce crystalline high aspect ratio nanowires of many different kinds of semiconductors, including Group II–VI, III–V, and IV materials and represents a general strategy for producing nanowires. In contrast to gas-phase VLS methods, which are limited to batch reactions on substrate surfaces, SLS nanowires growth can be used to produce large quantities of nanowires, as needed for applications like printed electronics and nanowires/polymer composites.

There may be a tradeoff in purity and yield of nanowires, and perhaps this will be one of the deciding factors about which nanowires growth method. Ge nanowires were also grown to use variety seed materials by Tuan *et al*[60]. All of the nanocrystals produced nanowires at temperatures significantly below their bulk eutectic temperatures. These nanocrystals most likely promote nanowire crystallization from solid-phase seeds. Solid phase metal-seeded nanowire growth has also been proposed in other systems. Solid-phase seeding is a viable growth mechanism, provided that the seed particles are small enough for rapid saturation by solid-state diffusion and the semiconductor has a high solid solubility in the metal. Co, Ni, Fe, and Cu all form alloys with Si and Ge at the growth temperatures and energy dispersive spectroscopy (EDS) analysis of the seed particles found at the tips of many nanowires revealed silicide and germanides. In the particles located at the tips of nanowires seeded with CuS and Fe_2O_3 nanocrystals, S and O were not observed in significant quantities, indicating that wires probably crystallize from copper silicide and iron germanide phases. Perhaps CuS and Fe_2O_3 are first reduced to Cu and Fe metal in the reaction mixture, prior to nanowire growth. Particles found at the tips of Fe,Pt-seeded nanowires showed all three elements — Fe, Pt, and Ge — indicating that nanowire growth probably originates from a ternary Fe:Pt:Ge phase. Perhaps the difference in nanowire growth direction relates to the solid-phase Au does not catalyze reactant decomposition, but simply helps drive crystallization (Au could be called a “crystallization catalyst”, but not a catalyst for reactant decomposition). In contrast to Au, the transition metals Ni, Co, and Fe, are catalysts for molecular decomposition reactions. For carbon nanotube (CNT) growth, Fe, Co, and Ni are used as catalysts that enhance reactant decomposition at the seed surface, while also promoting “crystallization” of the nanostructure for CNTs that is graphitization and tube growth. Au-seeded

CVD nanowire growth typically uses very reactive precursors, such as silane, and there is generally no need to use catalytic seed metals to promote reactant decomposition. However, sidewall deposition can occur with reactive precursors and lead to substantial diameter tapering over the length of the wire. Catalytic seeds might be able to lower the growth temperature and help prevent sidewall deposition. In Au seeded, solution-phase nanowire growth, many organosilane and organogermane reactants, such as octylsilane, are too unreactive to promote nanowire formation at typical reaction temperatures of the nanocrystals studied, Cobalt gave the highest yield and quality of both Si and Ge nanowires, rather than Au-seeded reactions. All growth temperatures were well below the bulk eutectic temperatures, indicating solid-phase seeding. Solid-phase seeding can probably occur for any semiconductor with a high solubility in the seed metal; however, the growth temperature must be sufficiently high for fast saturation by solid-state diffusion, which can occur relatively fast in nanometer-diameter seed particles. Cobalt was also found to catalyze silane decomposition to promote Si nanowire growth from octylsilane and trisilane, similar to past studies on Ni nanocrystals in gas-phase reactions, the use of catalytic transition-metal seeds might enable lower temperature reactions for less sidewall deposition and better diameter control. As more seed materials are studied, the solid-phase growth method may become as prevalent as liquid-eutectic seeding, and the use of catalytic seed particles might serve as a general approach for improved diameter control, as it has for carbon nanotube growth.

III. Experiment

3.1. Materials

All reagents and solvents were purchased from Alfa Aesar and Sigma Aldrich. Bismuth nanoparticles was mixed with above precursor solution with vigorous mixing and heated to 370ºC under Ar for 20min, and allowing it to cool to room temperature.

3.2. Instrumentations

Ge nanowires were synthesized under Ar in a three-neck flask on a Schlenk line after modifying by Fanfair *et al*[57]. A field-emission transition electron microscope (FE-TEM) (JEOL 2010F), operating at 200 KV, was used for investigating the microstructure of the sample. The field emission scanning electron microscopy (FE-SEM) was done using LEO 1530FE and NanoSem 230. Raman measurements were performed using a Renishaw 2000 Raman microscope system. A MellesGriot He-Ne laser operating at λ=632.8 nm was used as the excitation source with a laser power of approximately 30 mW. The Rayleigh line was removed from the collected Raman scattering using a charge-couled device (CCD) camera at a spectral resolution of 4 cm^{-1}. Each spectrum was accumulated three times with an exposure time of 30 seconds using ×50 objective lens. The anodes for the battery test cells were made of c-NW, super P carbon black, and polyvinylidone fluoride (PVDF) binder (Solef) in a weight ratio of 80:10:10. The slurry was prepared by thoroughly mixing an N-methyl-2-pyrrolidone (NMP) (Aldrich) solution of PVDF, carbon black, and the anode material. The coin-type half cells (2016R size), prepared in a Argon-filled glove box, contained an c-NW, a Li metal a microporous polyethylene separator, and an electrolyte solution of 1.05 M $LiPF_6$ in ethylene carbonate/dimethyl carbonate (EC/DMC) (1:1 vol. %) (LG Chem., Korea). The loading of pure active material was mg/cm^2. For conducting ex situ TEM analysis of the cycled samples (after charging(lithium dealloy)), the composite electrode was dissembled the cell, and dispersed in acetone with ultrasonic treatment.

3.3. Experimental method

$GeCl_4$ (Alfa, 99.9%) stored an Ar filled glovebox upon purchase. All Tri-n-octylphosphine (Tech. grade, Aldrich) and other solvents were used without further purification. A precursor solution of 4 g of $GeCl_4$ and 15 ml TOP was first prepared by stirring for 2 Hrs in the glovebox. Bi nanocrystals were prepared following the procedures described by Holze *et al*[61]. 0.02 g of Bi nanoparticles was mixed with above precursor solution with vigorous mixing and heated to 370°C under Ar for 20 min. and allowing it to cool to room temperature. The nanowires in the black precipitate were washed with $CHCl_3$ and ethanol for 5 times and centrifuged again to obtain a purified nanowires product. Obtained Nanowires was moved to tube furnace and pulled vacuum for 20 min, and refilled with Ar. After increasing the furnace temperature to 700 ℃, C_2H_2 was flown into the furnace at a flow rate of 4cc/min for 1h. After cooling to room temperature, color of the NW was observed to be black. Scheme 6 shows c-Ge NWs growth method. The anodes for the battery test cells were made of c-NW, super P carbon black, and polyvinylidone fluoride (PVDF) binder (Solef) in a weight ratio of 80:10:10. The slurry was prepared by thoroughly mixing an *N*-methyl-2-pyrrolidone (NMP) (Aldrich) solution of PVDF, carbon black, and the anode material. The coin-type half cells (2016R size), prepared in a helium-filled glove box, contained a c-NW, a Li metal, a microporous polyethylene separator, and an electrolyte solution of 1.05 M $LiPF_6$ in ethylene carbonate/dimethyl carbonate (EC/DMC) (1:1 vol. %) (LG Chem., Korea). The loading of pure active material was 6 mg/cm^2. For conducting ex situ TEM analysis of the cycled samples (after charging (lithium dealloy)), the composite electrode was dissembled the cell, and dispersed in acetone with ultrasonic treatment.

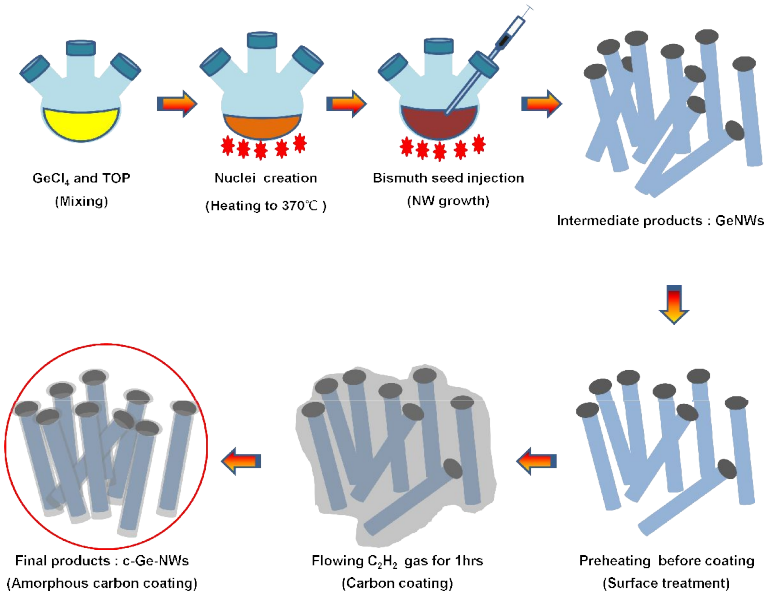

Scheme 6. Illustration of Ge nanowires growth method is used by as precursor $GeCl_4$ with Bi-seeds into TOP and amorphous carbon coating.

IV. Results and discussion

4.1. Scanning Electron microscopy

Figure 6 shows Ge NWs with a diameter of ~80nm produced by injecting $GeCl_4$ solution into the mixture of TOP (a capping ligand) and Bi nanoparticle seeds at 370°C in a three-necked flask on a Schlenk line. Figure 6(a) shows a photogragh of the entangled Ge NWs, and SEM image reveals a high quality Ge NWs with an average diameter of ~80 nm (Figure 6(d)). The wires were long and generally straight, the average length of the nanowires is greater than 10µm, and many are longer than 100 µm.

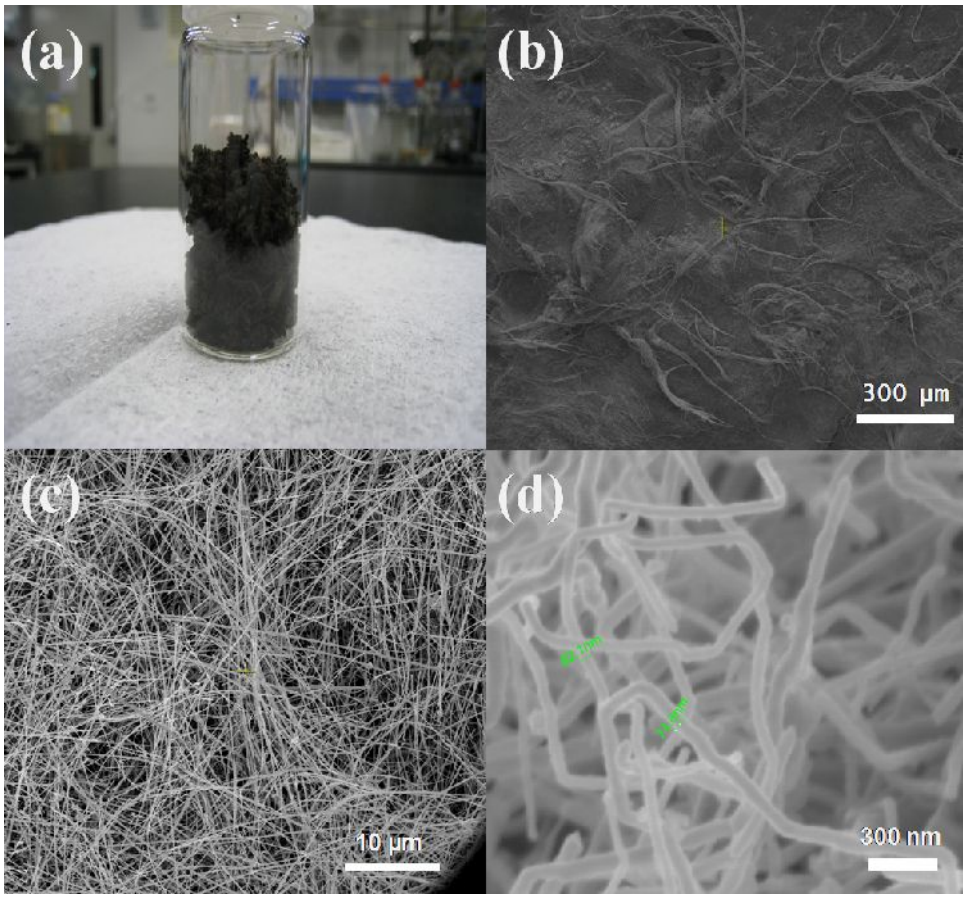

Figure 6. (a) The photogragh of Ge NWs in the vial, (b, c and d) SEM images of as-produced Ge NWs.

4.2. Transmission Electron Microscopy

Figure 8 shows a TEM images of the Bismuth nanoparticles, and the morphology of these is diffraction pattern. The particle size is below 20~30 nm and the shape is shown dependently as a circle.

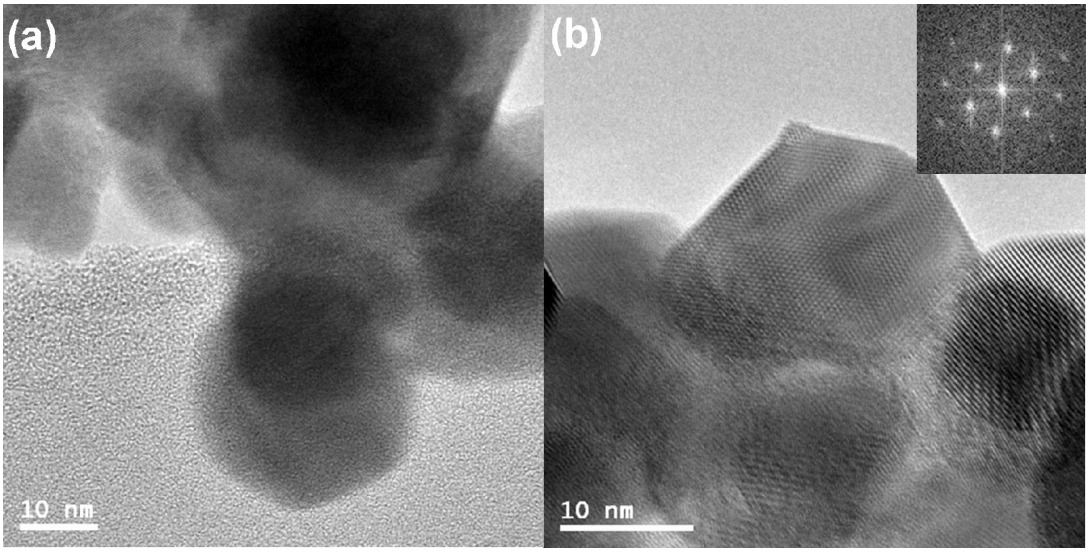

Figure 7. TEM images of Bismuth nanoparticles

Figure 9(a) shows a TEM image of the Ge nanowires, and the energy dispersive X-ray spectroscopy (EDAX) mapping of those wires is also presented in Figure 9(b-d). Bismuth nanoparticles-ended Ge NWs were clearly observed with EDXS mapping, and phosphorous was also detected on the Ge NWs. The HR-TEM image shows an amorphous coating layer with a thickness of 2 nm ~ 10 nm, and EDXS mapping supports that the coating layer is phosphorous in Figure 9(d). It seems that this layer originated from the decomposition of TOP during synthesis.

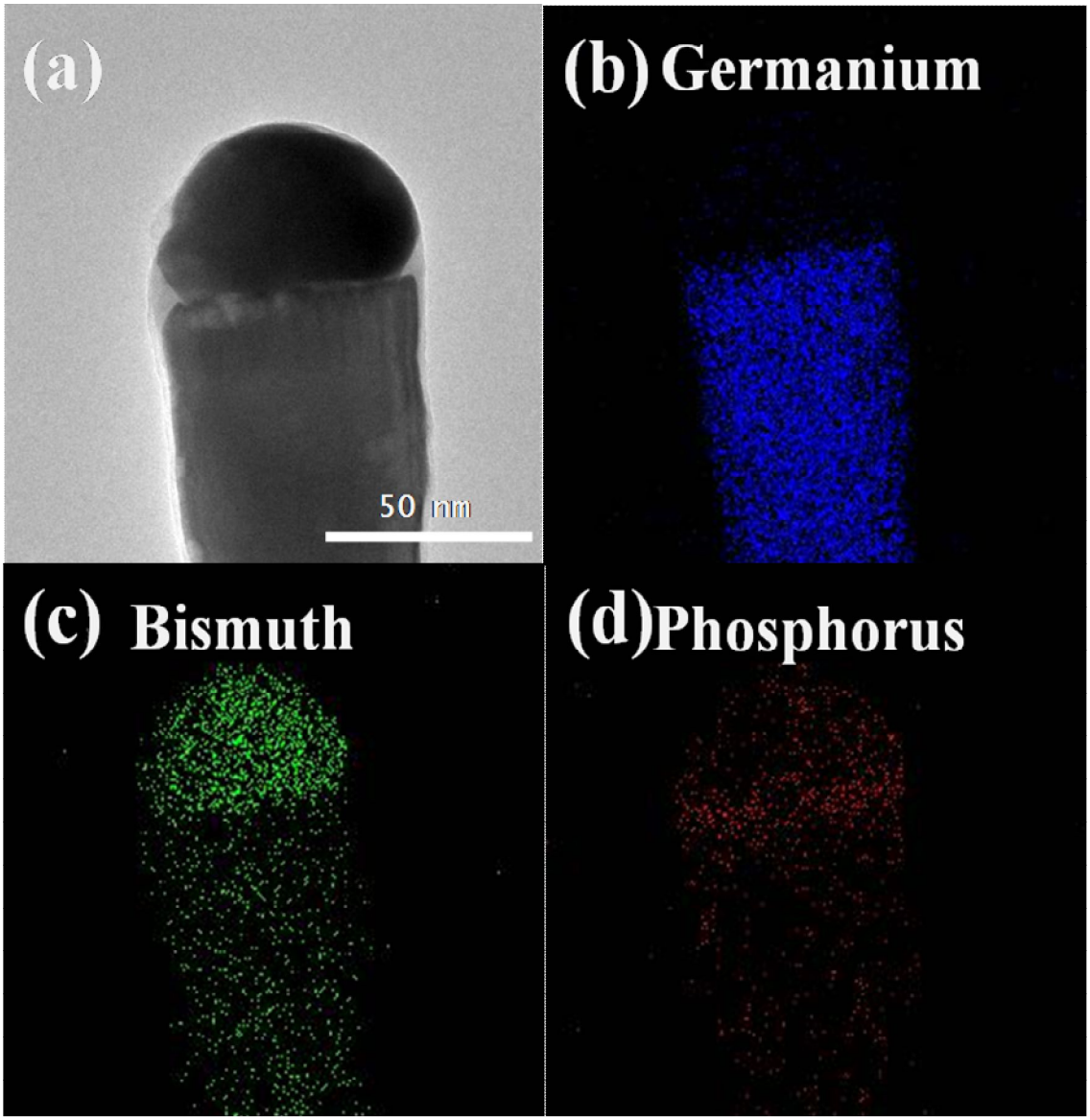

Figure 8. TEM images of Ge NW (b,c, and d) EDX mapping images of (a).

In order to enhance conductivity, carbon was also coated on the Ge NWs by decomposition of C_2H_2 gas at 700 ºC for 1h under an Argon atmosphere in tube furnace. The TEM image of the c-Ge-NWs shows that carbon is homogeneously coated on the Ge NWs with a thickness of ~20 nm, as can be seen in Figure 10(b). The amount of carbon in the c-Ge-NWs was 10 wt%, as measured by a CHS analyzer. EDXS line profiles also confirmed that there is a carbon layer on the surface of the Ge NWs and that P still remained after the carbon coating (Figure 10(c)). Nanoparticle powders are usually aggregated, and so nanoparticles become agglomerated and grow during the heating process for carbon coating, resulting in inhomogenous particle size and carbon coating. However, it is not easy for nanowires to aggregate in parallel because they are one dimensional, as shown in Figure 10(a) and Figure 10(b). Therefore, the agglomeration of nanowires is inhibited effectively during carbon coating, resulting in homogeneous carbon coating. Figure 10(d) exhibits the Raman spectrum of the c-Ge-

NWs, and two peaks were observed at ~1360 cm^{-1} and 1580 cm^{-1}indicating the D band and G band, respectively. The ratio of intensities, $I_{D\text{-}band}/I_{G\text{-}band}$, indicates the ordering degree of the carbon structure and the value for the fully ordered carbon is estimated to be 0.09. The relative peak area ratios and sharpness of the D and G band peaks depend on the crystallinity of the carbon materials, and a stronger D band and broad peaks indicate that amorphous carbon is coating on the Ge-NWs. Additionally, a peak at ~ 200 cm^{-1} was noticeable, which is indicative of Ge-Ge vibration. Also, even after carbon coating, GeO_x formation was not observed.

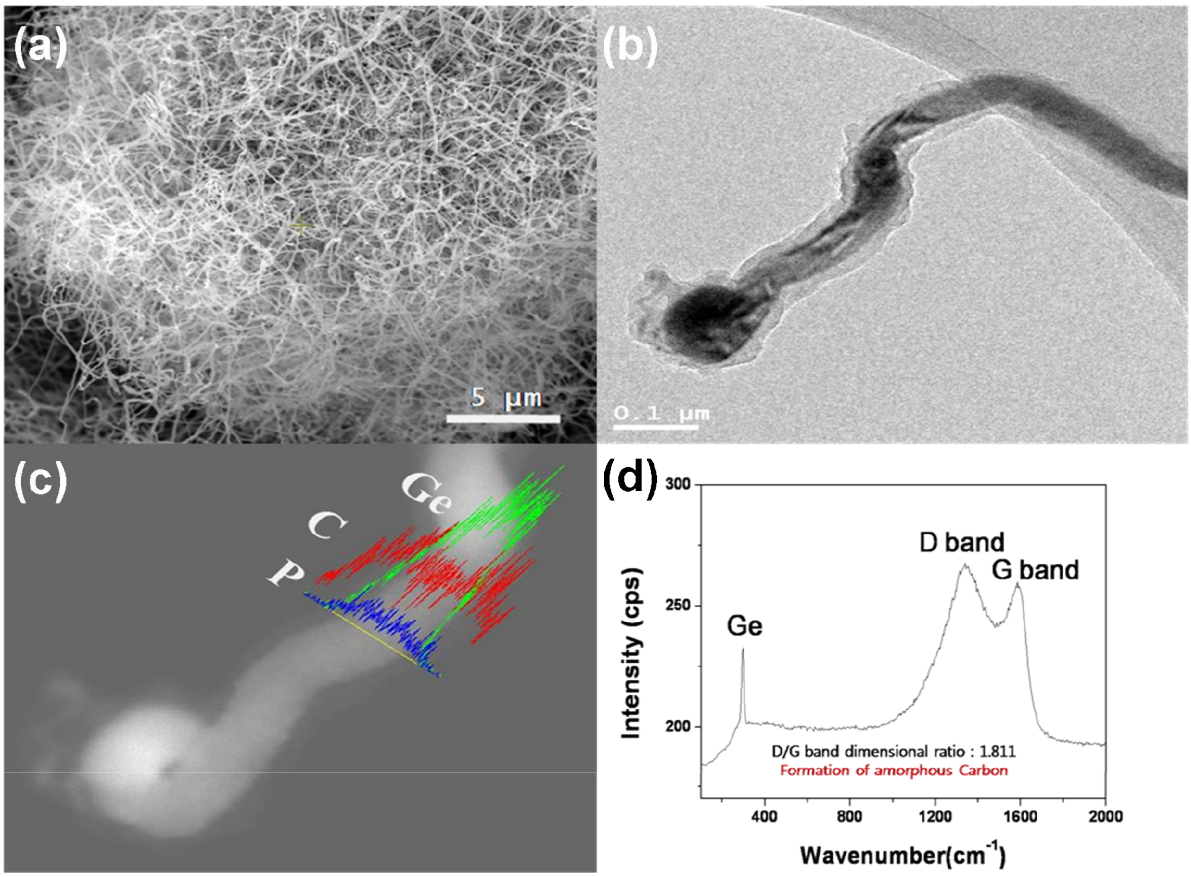

Figure 90. (a) SEM image and (b) TEM image of Ge-NWs after carbon coating, (c) EDS line profiles of Ge, C and P along the yellow line, and (d) Raman spectrum of c-Ge-NWs.

4.3. The change of morphology after cycling

Figure 11 is showed the morphology change of Ge NWs during cycles. Also, after 100 cycles, the diameter of the Ge NWs increased to 250 nm as result of lithium de/insertion, which about 4 times greater than the pristine sample (Figure 11 (b,e)). This means that Ge NWs have a quite porous structure (Figure 11 (f)). It is also noteworthy that the c-Ge-NWs were not cracked after cycling and that they preserved their own nanowires morphology, which contrasts with the reactions of Ge thin

films and nanoparticles to cycling.[38,41] The robustness of the c-Ge-NWs seems to be caused by avoiding a two phase reaction. Crystalline Ge NWs transformed into amorphous Ge NWs during cycling and amorphous Ge NWs experience a one phase reaction. Therefore, this material considerably suppresses local stress gradients through a homogenous volume change of electrode materials during electrochemical de/alloying, resulting in the inhibition of cracking and pulverization. In addition, Figure 11(c) is showed that Ge NWs are a single crystal by the Fourier transformed image. The transformation of crystalline Ge into amorphous Ge after cycling is also confirmed by the broad amorphous rings of the electron diffraction pattern in Figure 11(f).

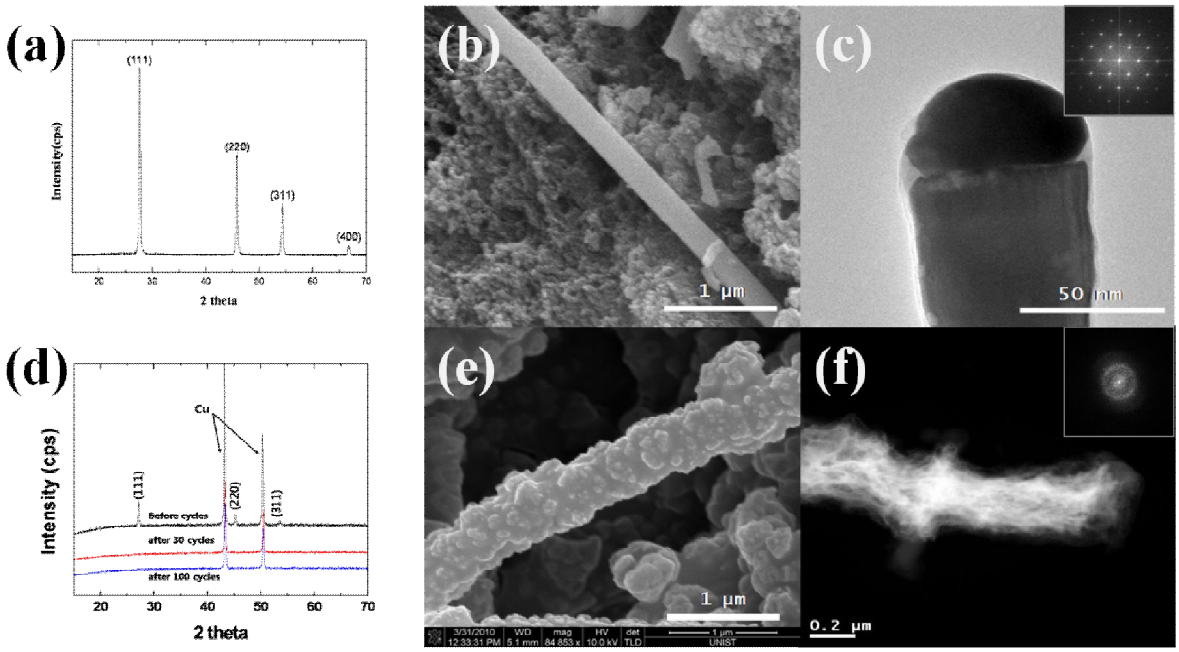

Figure 10. (a,d) XRD patterns of GeNWs before and after cycling , (b, c) SEM,TEM images of c-Ge-NWs Before cycling, (e,f) SEM,TEM images of c-Ge-NWs after cycling

4.4. Electrochemical Performance

Figure 12(a) exhibits the voltage profiles of the Ge NWs sheathed with amorphous carbon, and the discharge and charge capacity of the first cycle were 1053 mAh/g and 963 mAh/g in the range of 0 V and 1.5 V *vs*. Li/Li^+ at the rate of 0.5C (= 400 mA/g), which corresponds to a coulombic efficiency of 91%. This value is the highest yet reported for Ge nanoparticles and Ge NWs, and the coulombic efficiencies of previously reported Ge nanoparticles and Ge NWs were less than 75%. Differential capacity profiles of the 1st, 2nd, and 30th cycles are plotted in Figure 12(b). The peaks are indicative of lithium insertion into equipotential sites, and the presence of multiple sharp peaks at the first cycle suggests that a number of different Li-Ge phases be formed during electrochemical lithiation through a two-phase reaction. The broad peaks during lithium alloy process after the 2nd cycle indicates that Ge NWs experience a one-phase reaction, which is attributed to the formation of amorphous alloy or Ge. In crystalline Ge materials, it has been reported that crystalline intermetallic phases are usually formed on lithium insertion. This leads to enormous volume expansion, and causes high volume strain at interfaces, resulting in cracking and pulverization of materials. Therefore, some Ge materials may lose electrical contact from current collectors, and the reversible capacity fades on cycling. However, it was recently reported that an amorphous Ge phase is formed during cycling when Ge NWs are used as active materials, although the reason for this has not been clearly explained. Therefore, the stable cycle performance of c-Ge-NWs can be attributed to the formation of an amorphous Ge phase. Capacity retention after 100 cycles was 72% at the rate of 0.5C, as shown in Figure 12(c). For comparison, a Ge-C composite with a particle size of ~ 20 nm showed 76% capacity retention after 50 cycles at the rate of 0.1C. The rate capability of c-Ge-NWs for charging is shown in Figure 12(d). The charge capacities were 893 mAh/g, 843 mAh/g, 764 mAh/g, and 700 mAh/g at rates of 1C (=800 mA/g), 2C, 4C, and 6C (=4800 mA/g), respectively. The discharge rate was fixed at the 0.1C rate. These capacity values correspond to 93%, 88%, 80%, and 73% of the charge capacity at the 0.1C rate, respectively. For comparison, Ge NWs prepared by direct VLS growth on metallic current collectors delivered ~ 600 mAh/g at the 2C rate,[22] and c-Ge nanocomposite showed 613 mAh/g at 900 mA/g.[40] The improved rate performance is attributed to the morphology of the nanowires.

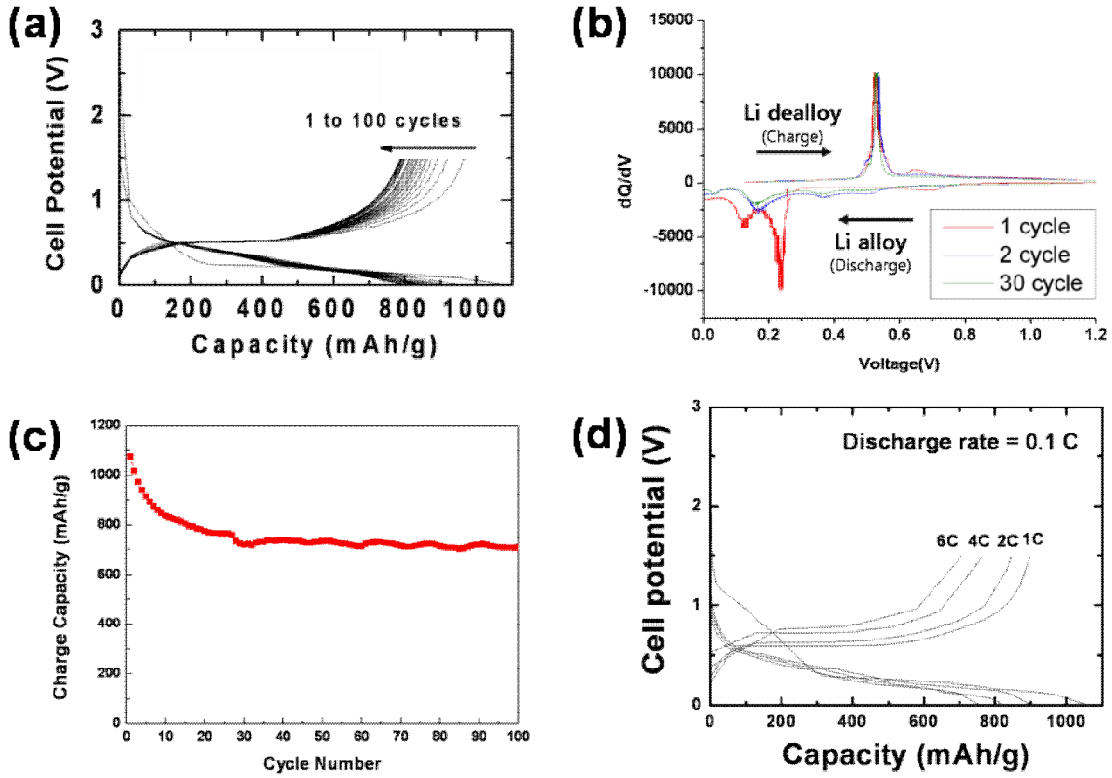

Figure 11. Electrochemcial performance of c-Ge-NW, Voltage profiles of c-Ge-NW at a 0.5C rate, (b) differential capacity plots of the 1st, 2nd and 30th cycles, (c) cycle performance of charge capacity, and (d) voltage profiles of c-Ge-NWs at the various C rate from 1 to 6 (discharge rate was fixed at 0.1C). All cells were examined at 21°C.

V. Conclusions

The composite electrode composed of single crystalline Ge NWs sheathed with amorphous carbon showed excellent electrochemical properties of large reversible capacity, high coulombic efficiency, excellent rate capability and stable cycle performance. The improved electrochemical performance of c-Ge-NWs fabricated in this experiment is attributed to the formation of amorphous Ge NWs during cycling, inhibition of surface oxidation of the Ge NWs and a homogenous carbon coating on discrete Ge NWs. These results suggest that the use of nanowire structure can be promising for alloy anode materials in lithium ion batteries.

Reference

1 CUI, L.-F., YANG, Y., HSU, C.-M. & CUI, Y. 2009. Carbon−Silicon Core−Shell Nanowires as High Capacity Electrode for Lithium Ion Batteries. *Nano Letters,* 9**,** 3370-3374.

2 NOH, M., KWON, Y., LEE, H., CHO, J., KIM, Y. & KIM, M. G. 2005. Amorphous Carbon-Coated Tin Anode Material for Lithium Secondary Battery. *Chemistry of Materials,* 17**,** 1926-1929.

3 PARK, M. H., KIM, K., KIM, J. & CHO, J. 2010. Flexible Dimensional Control of High-Capacity Li-Ion-Battery Anodes: From 0D Hollow to 3D Porous Germanium Nanoparticle Assemblies. *Advanced Materials,* 22**,** 415-418.

4 CHAN, C. K., ZHANG, X. F. & CUI, Y. 2007. High Capacity Li Ion Battery Anodes Using Ge Nanowires. *Nano Letters,* 8**,** 307-309.

5 NOH, M., KIM, Y., KIM, M. G., LEE, H., KIM, H., KWON, Y., LEE, Y. & CHO, J. 2005. Monomer-Capped Tin Metal Nanoparticles for Anode Materials in Lithium Secondary Batteries. *Chemistry of Materials,* 17**,** 3320-3324.

6 LEE, H., KIM, M. G., CHOI, C. H., SUN, Y.-K., YOON, C. S. & CHO, J. 2005. Surface-Stabilized Amorphous Germanium Nanoparticles for Lithium-Storage Material. *The Journal of Physical Chemistry B,* 109**,** 20719-20723.

7 ST. JOHN, M. R., FURGALA, A. J. & SAMMELLS, A. F. 1982. Thermodynamic Studies of Li-Ge Alloys: Application to Negative Electrodes for Molten Salt Batteries. *Journal of The Electrochemical Society,* 129**,** 246-250.

8 BOUKAMP, B. A., LESH, G. C. & HUGGINS, R. A. 1981. All-Solid Lithium Electrodes with Mixed-Conductor Matrix. *Journal of The Electrochemical Society,* 128**,** 725-729.

9 HUGGINS, R. A. 1998. Lithium alloy negative electrodes formed from convertible oxides. *Solid State Ionics,* 113-115**,** 57-67.

10 KASAVAJJULA, U., WANG, C. & APPLEBY, A. J. 2007. Nano- and bulk-silicon-based insertion anodes for lithium-ion secondary cells. *Journal of Power Sources,* 163**,** 1003-1039.

11 LI, H., WANG, Z., CHEN, L. & HUANG, X. 2009. Research on Advanced Materials for Li-ion Batteries. *Advanced Materials,* 21**,** 4593-4607.

12 KIM, M. G. & CHO, J. 2009. Nanocomposite of Amorphous Ge and Sn Nanoparticles as an Anode Material for Li Secondary Battery. *Journal of The Electrochemical Society,* 156**,** A277-A282.

13 KIM, M. G. & CHO, J. 2009. Reversible and High-Capacity Nanostructured Electrode Materials for Li-Ion Batteries. *Advanced Functional Materials,* 19**,** 1497-1514.

14 CUI, L.-F., RUFFO, R., CHAN, C. K., PENG, H. & CUI, Y. 2008. Crystalline-Amorphous Core−Shell Silicon Nanowires for High Capacity and High Current Battery Electrodes. *Nano Letters,* 9**,** 491-495.

15 KWON, Y., KIM, H., DOO, S.-G. & CHO, J. 2007. Sn0.9Si0.1/Carbon Core−Shell Nanoparticles for High-Density Lithium Storage Materials. *Chemistry of Materials,* 19**,** 982-986.

16 KIM, C., NOH, M., CHOI, M., CHO, J. & PARK, B. 2005. Critical Size of a Nano SnO2 Electrode for Li-Secondary Battery. *ChemInform,* 36**,** no-no.

17 KIM, E., SON, D., KIM, T. G., CHO, J., PARK, B., RYU, K. S. & CHANG, S. H. 2004. A Mesoporous/Crystalline Composite Material Containing Tin Phosphate for Use as the Anode in Lithium-Ion Batteries. *Angewandte Chemie,* 116**,** 6113-6116.

18 CHAN, C. K., PENG, H., LIU, G., MCILWRATH, K., ZHANG, X. F., HUGGINS, R. A. & CUI, Y. 2008. High-performance lithium battery anodes using silicon nanowires. *Nat Nano,* 3**,** 31-35.

19 TRENTLER, T. J., HICKMAN, K. M., GOEL, S. C., VIANO, A. M., GIBBONS, P. C. & BUHRO, W. E. 1995. Solution-Liquid-Solid Growth of Crystalline III-V Semiconductors: An Analogy to Vapor-Liquid-Solid Growth. *Science,* 270**,** 1791-1794.

20 WAGNER, R. S. & ELLIS, W. C. 1964. VAPOR-LIQUID-SOLID MECHANISM OF

SINGLE CRYSTAL GROWTH. *Applied Physics Letters,* 4**,** 89-90.
21 MORALES, A. M. & LIEBER, C. M. 1998. A laser ablation method for the synthesis of crystalline semiconductor nanowires. *Science,* 279**,** 208-211.
22 KORNOWSKI, A., GIERSIG, M., VOGEL, R., CHEMSEDDINE, A. & WELLER, H. 1993. Nanometer-sized colloidal germanium particles: Wet-chemical synthesis, laser-induced crystallization and particle growth. *Advanced Materials,* 5**,** 634-636.
23 WU, Y. & YANG, P. 2000. Germanium Nanowire Growth via Simple Vapor Transport. *Chemistry of Materials,* 12**,** 605-607.
24 WOLFENSTINE, J. 1999. Critical grain size for microcracking during lithium insertion. *Journal of Power Sources,* 79**,** 111-113.
25 KIM, H. & CHO, J. 2008. Superior Lithium Electroactive Mesoporous Si@Carbon Core−Shell Nanowires for Lithium Battery Anode Material. *Nano Letters,* 8**,** 3688-3691.
26 KIM, H. & CHO, J. 2008. Hard templating synthesis of mesoporous and nanowire SnO2 lithium battery anode materials. *Journal of Materials Chemistry,* 18**,** 771-775.
27 CHO, J. 2010. Porous Si anode materials for lithium rechargeable batteries. *Journal of Materials Chemistry,* 20**,** 4009-4014.
28 MAO, O., TURNER, R. L., COURTNEY, I. A., FREDERICKSEN, B. D., BUCKETT, M. I., KRAUSE, L. J. & DAHN, J. R. 1999. Active/Inactive Nanocomposites as Anodes for Li-Ion Batteries. *Electrochemical and Solid-State Letters,* 2**,** 3-5.
29 YANG, J., WACHTLER, M., WINTER, M. & BESENHARD, J. O. 1999. Sub-Microcrystalline Sn and Sn-SnSb Powders as Lithium Storage Materials for Lithium-Ion Batteries. *Electrochemical and Solid-State Letters,* 2**,** 161-163.
30 BESENHARD, J. O., YANG, J. & WINTER, M. 1997. Will advanced lithium-alloy anodes have a chance in lithium-ion batteries? *Journal of Power Sources,* 68**,** 87-90.
31 WINTER, M. & BESENHARD, J. O. 1999. Electrochemical lithiation of tin and tin-based intermetallics and composites. *Electrochimica Acta,* 45**,** 31-50.
32 DEY, A. N. 1971. Electrochemical Alloying of Lithium in Organic Electrolytes. *Journal of The Electrochemical Society,* 118**,** 1547-1549.
33 FULLER, C. S. & SEVERIENS, J. C. 1954. Mobility of Impurity Ions in Germanium and Silicon. *Physical Review,* 96**,** 21.
34 GRAETZ, J., AHN, C. C., YAZAMI, R. & FULTZ, B. 2004. Nanocrystalline and Thin Film Germanium Electrodes with High Lithium Capacity and High Rate Capabilities. *Journal of The Electrochemical Society,* 151**,** A698-A702.
35 YANG, L. C., GAO, Q. S., LI, L., TANG, Y. & WU, Y. P. 2010. Mesoporous germanium as anode material of high capacity and good cycling prepared by a mechanochemical reaction. *Electrochemistry Communications,* 12**,** 418-421.
36 LEE, H., KIM, H., DOO, S.-G. & CHO, J. 2007. Synthesis and Optimization of Nanoparticle Ge Confined in a Carbon Matrix for Lithium Battery Anode Material. *Journal of The Electrochemical Society,* 154**,** A343-A346.
37 CUI, G., GU, L., ZHI, L., KASKHEDIKAR, N., AKEN, P. A. V., M LLEN, K. & MAIER, J. 2008. A Germanium-Carbon Nanocomposite Material for Lithium Batteries. *Advanced Materials,* 20**,** 3079-3083.
38 HWA, Y., PARK, C.-M., YOON, S. & SOHN, H.-J. 2010. The effect of Cu addition on Ge-based composite anode for Li-ion batteries. *Electrochimica Acta,* 55**,** 3324-3329.
39 CHEVALIER, P. Y. 1989. A thermodynamic evaluation of the Au-Ge and Au-Si systems. *Thermochimica Acta,* 141**,** 217-226.
40 GIVARGIZOV, E. I. 1975. Fundamental aspects of VLS growth. *Journal of Crystal Growth,* 31**,** 20-30.
41 WU, Y., CUI, Y., HUYNH, L., BARRELET, C. J., BELL, D. C. & LIEBER, C. M. 2004. Controlled Growth and Structures of Molecular-Scale Silicon Nanowires. *Nano Letters,* 4**,** 433-436.
42 WESTWATER, J., GOSAIN, D. P. & USUI, S. 1998. Si Nanowires Grown via the Vapour-Liquid-Solid Reaction. *physica status solidi (a),* 165**,** 37-42.
43 BUHRO, W. E., HICKMAN, K. M. & TRENTLER, T. J. 1996. Turning down the heat on

semiconductor growth: Solution-chemical syntheses and the solution-liquid-solid mechanism. *Advanced Materials,* 8**,** 685-688.

44 HEATH, J. R. & LEGOUES, F. K. 1993. A liquid solution synthesis of single crystal germanium quantum wires. *Chemical Physics Letters,* 208**,** 263-268.

45 WANG, D. & DAI, H. 2002. Low-Temperature Synthesis of Single-Crystal Germanium Nanowires by Chemical Vapor Deposition. *Angewandte Chemie International Edition,* 41**,** 4783-4786.

46 CHAMBREAU, S. D. & ZHANG, J. 2002. GeH_x (x=0-3) and Ge_nH_x (n=2-7) in flash pyrolysis of GeH₄. *Chemical Physics Letters,* 351**,** 171-177.

47 ERCOLESSI, F., ANDREONI, W. & TOSATTI, E. 1991. Melting of small gold particles: Mechanism and size effects. *Physical Review Letters,* 66**,** 911.

48 JAGANNATHAN, H., DEAL, M., NISHI, Y., KIM, H.-C., FREER, E. M., SUNDSTROM, L., TOPURIA, T. & RICE, P. M. 2006. Templated germanium nanowire synthesis using oriented mesoporous organosilicate thin films. *Journal of Vacuum Science & Technology B: Microelectronics and Nanometer Structures,* 24**,** 2220-2224.

49 HANNON, J. B., KODAMBAKA, S., ROSS, F. M. & TROMP, R. M. 2006. The influence of the surface migration of gold on the growth of silicon nanowires. *Nature,* 440**,** 69-71.

50 LENSCH-FALK, J. L., HEMESATH, E. R., LOPEZ, F. J. & LAUHON, L. J. 2007. Vapor−Solid−Solid Synthesis of Ge Nanowires from Vapor-Phase-Deposited Manganese Germanide Seeds. *Journal of the American Chemical Society,* 129**,** 10670-10671.

51 SUN, X., CALEBOTTA, G., YU, B., SELVADURAY, G. & MEYYAPPAN, M. 2007. Synthesis of germanium nanowires on insulator catalyzed by indium or antimony. *Journal of Vacuum Science & Technology B: Microelectronics and Nanometer Structures,* 25**,** 415-420.

52 CHEVALIER, P. Y. 1988. Thermodynamic evaluation of the Bi-Ge system. *Thermochimica Acta,* 132**,** 111-116.

53 YAN, C. & LEE, P. S. 2009. Bismuth-Catalyzed Growth of Germanium Nanowires in Vapor Phase. *The Journal of Physical Chemistry C,* 113**,** 2208-2211.

54 XIANG, Y., CAO, L., ARBIOL, J., BRONGERSMA, M. L. & FONTCUBERTA I MORRAL, A. 2009. Synthesis parameter space of bismuth catalyzed germanium nanowires. *Applied Physics Letters,* 94**,** 163101.

55 HANRATH, T. & KORGEL, B. A. 2002. Nucleation and Growth of Germanium Nanowires Seeded by Organic Monolayer-Coated Gold Nanocrystals. *Journal of the American Chemical Society,* 124**,** 1424-1429.

56 LU, X., FANFAIR, D. D., JOHNSTON, K. P. & KORGEL, B. A. 2005. High Yield Solution−Liquid−Solid Synthesis of Germanium Nanowires. *Journal of the American Chemical Society,* 127**,** 15718-15719.

57 FANFAIR, D. D. & KORGEL, B. A. 2005. Bismuth Nanocrystal-Seeded III-V Semiconductor Nanowire Synthesis. *Crystal Growth & Design,* 5**,** 1971-1976.

58 CHOCKLA, A. M. & KORGEL, B. A. 2009. Seeded germanium nanowire synthesis in solution. *Journal of Materials Chemistry,* 19**,** 996-1001.

59 PAN, Z. W., DAI, S. & LOWNDES, D. H. 2005. Straight single-crystalline germanium nanowires and their patterns grown on sol-gel prepared gold/silica substrates. *Solid State Communications,* 134**,** 251-255.

60 TUAN, H.-Y., LEE, D. C. & KORGEL, B. A. 2006. Nanocrystal-Mediated Crystallization of Silicon and Germanium Nanowires in Organic Solvents: The Role of Catalysis and Solid-Phase Seeding. *Angewandte Chemie International Edition,* 45**,** 5184-5187.

61 HOLZE, R. 2005. Lithium batteries: science and technology, Gholam-Abbas Nazri and Gianfranco Pistoa (eds). *Journal of Solid State Electrochemistry,* 9**,** 794-795.